

Nanostructure morphology influences in electrical properties of titanium dioxide thin films

Patrick Pires Conti^{1,2}, Eupídio Scopel^{1,3}, Edson Roberto Leite^{2,b)}, Cleocir José Dalmaschio^{1,a)} 

¹Department of Chemistry, Federal University of Espírito Santo (UFES), Vitória 29075-910, Espírito Santo, Brazil

²Department of Chemistry, Federal University of São Carlos (UFSCar), 13565-905, São Carlos, São Paulo, Brazil

³Department of Physical Chemistry, Institute of Chemistry, University of Campinas (Unicamp), 13083-970, Campinas, São Paulo, Brazil

^{a)}Address all correspondence to this author. e-mail: cleocir.dalmaschio@ufes.br

^{b)}Contributing Editor: Edson Leite

Received: 17 April 2020; accepted: 3 August 2020

Titanium dioxide (TiO₂) is a semiconductor that can be applied in different technological areas. In this work, we investigated the modifications of the electrical properties of thin films composed of TiO₂ nanoparticles produced with different morphologies. The solvothermal route used for the synthesis allowed the production of nanoparticles with functionalized surfaces due to oleate groups. It was possible to modulate nanocrystals shape and size due to the detachment crystal growth mechanism, by changing the reaction time. Nanorods were obtained using 4 h of synthesis, and an increase in the reaction time to 64 h led to a bipyramidal morphology. The functionalization by the organic ligand allowed the preparation of stable colloidal solutions, which were used to prepare thin films by the dip-coating method. The films presented a homogeneous surface, an average thickness around 100 nm, and no agglomerations were observed. The electrical resistance measurements indicated a typical behavior of semiconductors, and they were dependent on the nanoparticle morphology. An exploratory test indicated that the thin films prepared using nanorod particles presented a higher electrical response compared with isotropic particles, when exposed in a liquefied petroleum gas vapor atmosphere. Therefore, the morphology of the nanoparticles is a key factor for the further application of these thin films in gas sensing. Employing an easy methodology which required simple apparatus, and by using reaction time modulation only, it was possible to prepare homogeneous thin films with a tunable electrical response.

Introduction

Titanium dioxide (TiO₂) is a nontoxic, low cost, and photocorrosion-free semiconductor that is used in several technological applications, such as dye-sensitized solar cells [1, 2], photoelectrochemistry [3], photocatalysis [4, 5, 6], and sensors [7, 8]. These applications are achievable mainly due to the electrical conductivity and the photocatalytic properties [9, 10] of TiO₂ which are enhanced at the nanometric scale.

The outstanding properties of TiO₂ make it an interesting material for use as a sensing element in electronic devices, such as gas sensors [11]. An electronic sensor consists of a substrate, an electrode, and a sensing element, which can be a thin film of semiconductor material, such as TiO₂. The interaction of the sensing element with gases is reversible [12] and is affected by the surface area, the microstructure of sensing layers, and the temperature [13]. This promotes the use of

nanoparticles for the development of more robust gas sensors, with lower detection limits, better selectivity, shorter response, and recovery times [14]. For example, toxic gases monitoring such as liquefied petroleum gas (LPG) can be used to avoid health problems and prevent potential explosions [15, 16]. Thus, an adequate route to nanoparticle synthesis can be useful to improve the properties where TiO₂ is applied, for example, nanoparticles can be used as a sensing layer in electronic devices.

TiO₂ nanoparticles can be produced by several synthesis approaches, such as hydrothermal [17] and solvothermal [18] routes, deposition processes such as chemical vapor [19] or spray pyrolysis [20], and the sol-gel method [21]. The solvothermal route is a promising alternative to produce inorganic oxide nanocrystals with refined properties [22]. Nanoparticles of titanium oxide [23], zirconium oxide [24], and magnetite

[25] were successfully prepared by this route with uniformity in size and shape. In the process of crystal nucleation and growth, the nanoparticles present high surface energy. Thus, the use of surfactant molecules is necessary to act as a ligand on the nanocrystal surface resulting in a steric hindrance that will prevent disordered growth and excessive agglomeration. These molecules remain attached to the nanoparticles after synthesis [26]. For this reason, the inorganic oxides can be dispersed in organic solvents to form stable colloidal solutions which can facilitate the process of the nanoparticle deposition, targeting potential applications [27].

For TiO₂ synthesis, an organometallic, an alkoxide, or another coordination compound can be used as a metal precursor [28]. Fan et al. [29], aiming at obtaining TiO₂ nanostructures, employed tetrabutyl titanate, ethyl alcohol, and glycerol as chemical reagents in solvothermal reactions at 140, 170, and 200 °C for 24 h. The variation of the reaction temperature allowed the authors to obtain controlled crystallinity, band gap, crystallite size, and different morphologies of particles that were successfully used in the photocatalytic process.

Unlike the other methods used to synthesize TiO₂ nanoparticles, the solvothermal route has the advantage of allowing the modulation of the size and shape of the crystals by changing the reaction parameters. Previously, we observed that the use of the solvothermal route to synthesize TiO₂ nanoparticles led to an unusual phenomenon, in which nanorod structures evolve into bipyramid nanocrystals, in a process similar Rayleigh instability [18]. TiO₂ nanoparticles synthesized at short reaction times (0.25–4 h) have a predominately nanorod shape, whereas an increase in the reaction time (64 h) led to a reduction of the nanorods length, as a result of the detachment process, forming isotropic shapes for TiO₂ anatase as a bipyramidal structure.

Physical and chemical depositions are the two most common methods to obtain thin films. The film's formation and morphology are influenced by several factors, including the size and shape of the nanoparticles [30]. The evaporation technique is the commonest one based on physical deposition. Basically, the material in the solid phase is evaporated from a precursor material and further converted and deposited when in contact with the target surface [31]. In general, physical techniques result in films with remarkable properties. However, the use of sophisticated equipment makes the process expensive.

An alternative method to prepare thin films is the dip-coating technique, which is classified as a chemical deposition method used to obtain films that present good surface quality and thin thickness [32]. The films that are obtained by this method can be successfully used in technological applications such as gas sensors [33]. For this, it is necessary to control the nanoparticle morphology and to investigate how the

nanoparticles influence both the electrical and the gas-sensing performances.

Therefore, in this work, we used the solvothermal route for modulating the size and shape of TiO₂ nanoparticles by changing the reaction time (4, 16, and 64 h), employing only oleic acid and titanium (IV) butoxide. The obtained colloidal solutions were used to prepare thin films which presented properties dependent on the nanoparticle morphology. The nanoparticles and the thin films were characterized with regards to the morphology, crystalline structure, and electrical properties, besides exploratory tests of the electrical properties of the films with LPG vapor/air mixtures.

Results and Discussion

TiO₂ nanoparticles

The solvothermal route was efficient in the preparation of stable colloidal solutions in toluene, as shown in Fig. 1. An increase in the reaction time led to a difference in the color of the dispersions, which is associated with the oxidation of the organic chain [34]. TiO₂ nanoparticles were obtained in the pure anatase phase (PDF#21-1272) according to X-ray diffraction (XRD) analysis (Fig. 2). The nanoparticle crystallite size, synthesized at different times (4, 16, and 64 h), were calculated by the Scherrer equation [35] for certain crystallographic directions (Table 1). The values indicated a reduction in the size of the (004) direction with increasing reaction time. Morphological analysis [Figs. 3(a)–3(c)] corroborates the differences observed in XRD analysis by changing the shape of the nanoparticles. Nanoparticles submitted to 4 h of reaction time had a rod-like shape, while the nanoparticles synthesized using a longer reaction time, 64 h, were more isotropic, having a truncated bipyramidal shape.

This crystallization mechanism was previously described by Dalmaschio and Leite [18] and justified as a detachment

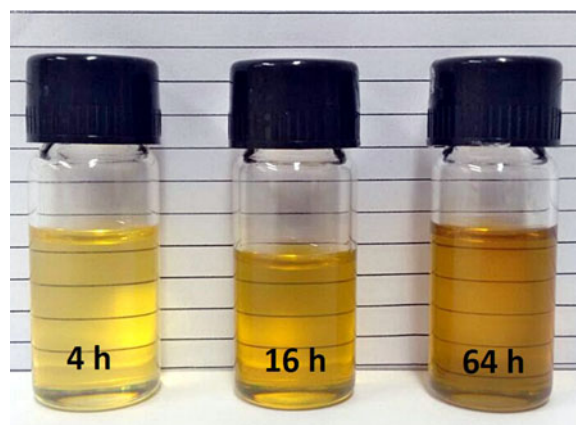


Figure 1: Functionalized TiO₂ nanocrystals in colloidal solution.

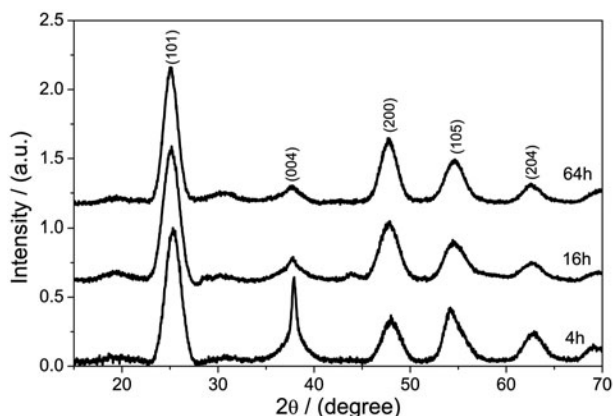


Figure 2: XRD pattern of the TiO₂ nanoparticles (indexed with the PDF#21-1272).

TABLE 1: Crystallite size calculated with the Scherrer equation for TiO₂ nanoparticles as synthesized and in thin film (thin films were thermally treated at 500 °C).

Sample	Size in each crystallographic direction (nm)				
	(101)	(004)	(200)	(105)	(204)
As synthesized					
4 h	4.15	12.1	3.68	6.83	3.43
16 h	4.09	4.79	3.57	5.75	3.51
64 h	4.09	2.75	4.16	5.93	3.46
Thin film (500 °C)					
4 h	10.3	13.8	19.0	31.6	7.08
64 h	11.1	14.6	20.3	31.3	6.43

process, similar to Rayleigh instability. At the beginning of the reaction, some nanocrystals interact by an oriented attachment process forming nanorods particles. An increase in the reaction time leads to crystal growth by mass transportation, resulting in dumbbell-shaped nanostructures. For longer times of reaction (64 h), a process similar to the Rayleigh instability promotes the fragmentation of the nanorods by a detachment of the crystals, which results in particles that present a truncated bipyramidal shape.

Indeed, the nanoparticles synthesized using 4 and 16 h of reaction were more anisotropic and presented largest average length than the nanoparticles synthesized using 64 h of reaction, which were more isotropic and presented a narrow size distribution [Figs. 3(d)–3(f)]. Therefore, the use of different times of reaction enables the modulation of the size and shape of the nanoparticles. This size polydispersion in nanoparticles can be used in the preparation of thin films to promote different surface areas. Thus, the nanoparticles can directly influence the detection of analytes, which are desirable tunable properties for gas monitoring sensitivity and selectivity [36].

The preparation of thin films also depends on an adequate dispersion of the nanoparticles in a solvent for further deposition on a substrate. The presence of an organic solvent in the synthesis allows the control of the particle morphology and the dispersion in an organic solvent (Fig. 1). The Fourier-transform infrared (FTIR) spectra (Fig. 4) indicate the presence of the oleate molecules in the nanoparticle surface resulting from the oleic acid deprotonation (C–H vibration at 2879 cm⁻¹ and C=O vibration

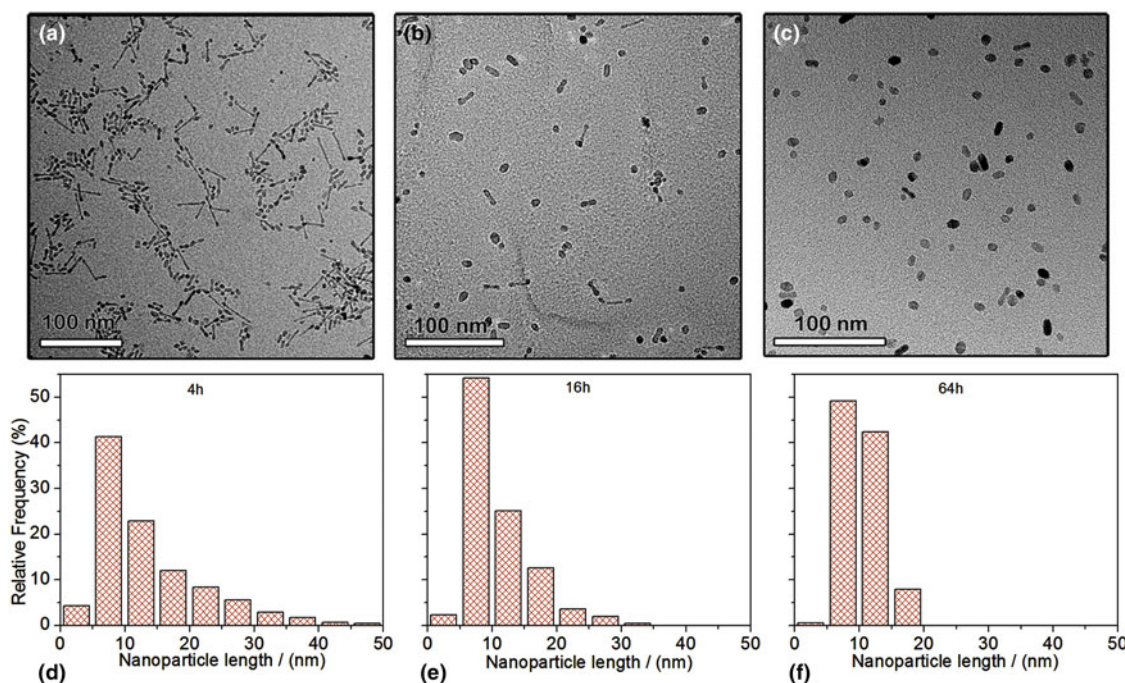


Figure 3: TEM images and particle size distribution: (a and d) 4 h, (b and e) 16 h, and (c and f) 64 h.

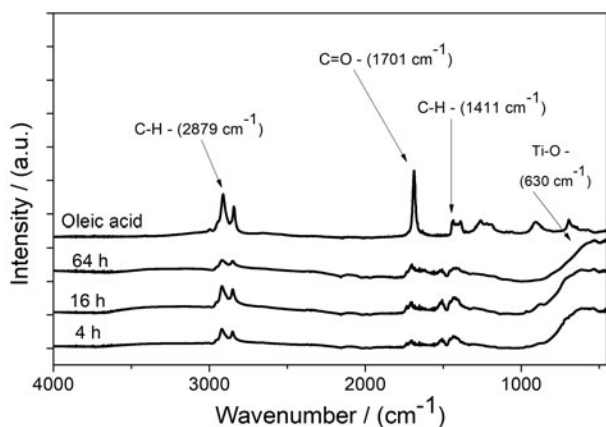


Figure 4: FTIR spectra of synthesized oxides and oleic acid.

at 1701 cm^{-1}). Also, Ti–O bond vibration is observed (between 630 and 650 cm^{-1}), which evidences the oxide formation [37]. Thus, the functionalization of the nanoparticle surface with oleate molecules is a key factor for the application of these nanoparticles as thin films. The solvent acts as a hindrance to the disordered agglomeration of the nanoparticles, which preserves the shape and size, and allows an efficient preparation of colloidal solutions [23].

Morphological and electrical properties of TiO₂ thin films

The colloidal solutions obtained from nanorods (4 h of synthesis) and bipyramids (64 h of synthesis) were chosen for an investigation of the influence of the morphology on the properties of the thin film. These two morphologies are significantly different from each other and could result in thin films with distinct responses. The thin films were deposited on glass substrates by a dip-coating method using the colloidal solutions (5 wt%). A sequential thermal treatment at $500\text{ °C}/2\text{ h}$ was applied, and the nanoparticles remained in the anatase phase without transition to another crystalline structure, as presented in Fig. 5. Also, the thermal treatment did not alter the particle

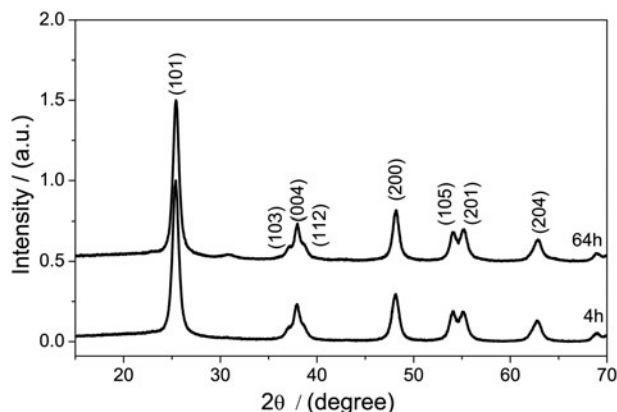


Figure 5: XRD pattern of the TiO₂ thin films after thermal treatment (indexed with the PDF#21-1272).

dimensions, maintaining the nanometer scale, as presented in Table 1. Comparing the crystal size before and after thermal treatment, it is evident how the crystals' growth occurred in all crystallographic directions. The morphological analysis performed by scanning electron microscopy (SEM) indicated homogeneity and continuity in the films' structure, without the presence of cracks or agglomerates (Fig. 6). The average thickness of the cross section of 4 h thin film was $109 \pm 6\text{ nm}$.

To evaluate whether NP's morphology affects the electronic mobility process, current–voltage curves at different temperatures, as shown in Figs. 7(a) and 7(b), were carried out. The *I*–*V* curve of the as-fabricated NPs' thin film showed typical behavior of semiconductors: an increase in temperature resulted in a decrease of the electrical resistance. Exploring the data, it is possible to see, in Figs. 7(c) and 7(d), a reduction in the electrical resistance when different temperature levels were applied. Using Eq. (2), the resistivity values of the films are 1.95 and $3.26\text{ }\Omega\text{ cm}$ for the 4 and 64 h thin films, respectively. Tang et al. conducted a thermal treatment of TiO₂ anatase thin films at 450 °C and found resistivity values in the same range, 10^0 – $10^1\text{ }\Omega\cdot\text{cm}$, as found in this work [38].

These electrical properties indicate the possibility of using these thin films as the sensitive element in gas sensors. For

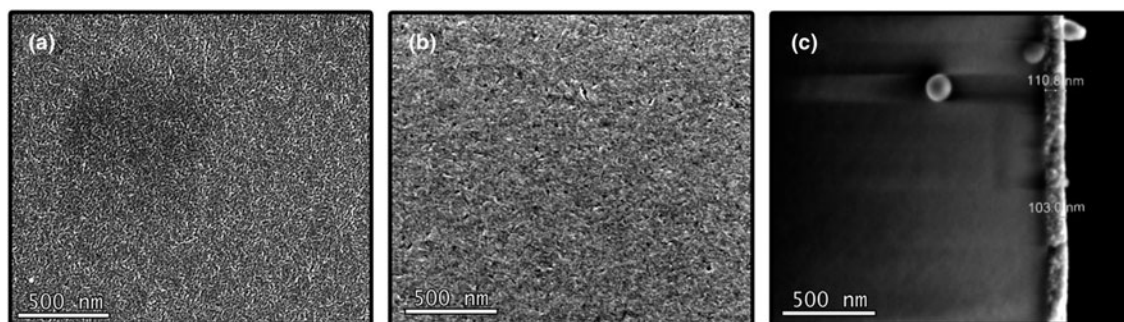


Figure 6: SEM images of thin films: (a) superior view, 4 h, (b) superior view, 64 h, and (c) cross section, 4 h.

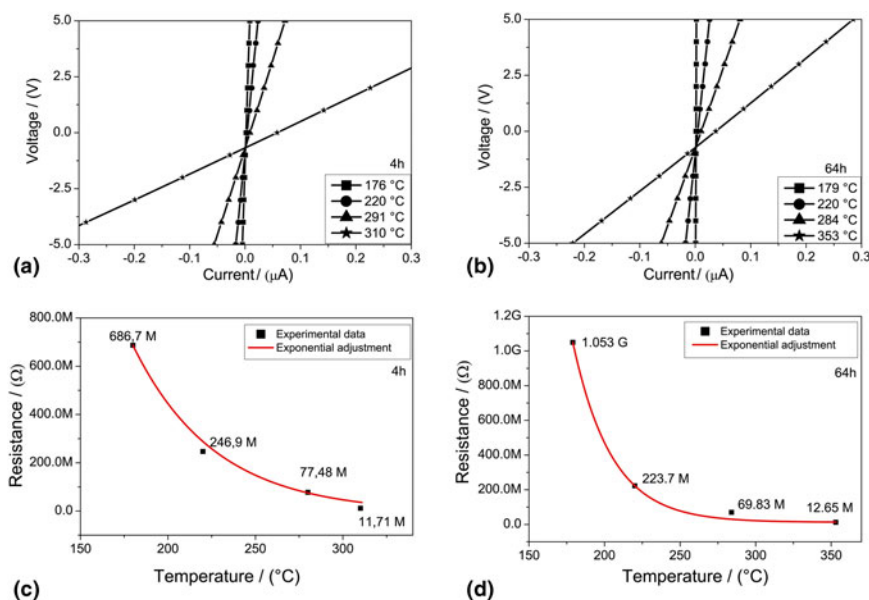


Figure 7: Current–voltage curves (a) 4 h and (b) 64 h. Values of electrical resistance with different temperatures (c) 4 h and (d) 64 h.

this, measurements at 350 °C, using concentrations of LPG vapor/air mixture (1127, 2774, and 6673 ppm), were performed (Fig. 8). Norms specified by National Institute for Occupational Safety and Health (NIOSH) and Occupational Safety and Health Administration (OSHA), the permissible exposure limit for LPG is 1000 ppm and the lower explosive limit is 21,000 ppm for propane and 19,000 ppm for butane [39]. In contact with the target analyte, both platforms responded by increasing the electrical resistance [Figs. 8(a) and 8(b)], showing isolated peaks at the beginning of the measurements as a result of the input gas mixture flux. These increases in resistance indicate that the gas was able to remove electrons from the conduction band of the oxide [40]. In the presence of LPG, the oxygen molecules form negatively charged oxygen ions (O^{2-} , O^- , and O_2^-) which are adsorbed on the TiO_2 surface and are responsible for electron recombination within the grain boundaries increasing the electrical resistance, as observed [41].

The effect of morphology on the LPG injection is associated with the exposed surface area, vacancies on crystalline lattice, and surface sites [42]. TiO_2 is a well-known intrinsic n-type semiconductor, but Ti vacancies (V_{Ti}) can result in p-type conductivity behavior [43]. Therefore, TiO_2 thin films with V_{Ti} should present an increase in electrical resistance when exposed to reducing agents. Correlating the data of electrical response and gas-sensitive properties [Fig. 8(c)], the film based on 4 h nanoparticles exhibited a higher response to the measuring gas. The crystal morphology before the deposition can be associated with the observed porosity because the rod-like shape promotes the production of films with more porosity, as observed by ellipsometry. The density determined for films deposited onto the silicon substrate and analyzed by

ellipsometry shows a value of 3.38 g/cm^3 for the film deposited using TiO_2 synthesized over 4 h, and 3.46 g/cm^3 for the material synthesized over 64 h.

The electrical response obtained from the film is more pronounced in the case of the 4 h film [Fig. 8(c)], which presented a higher porosity and a lower density. Therefore, the morphology of the nanoparticles can impact the film structure by interfering in the device sensing mechanism. Isotropic particles can be accommodated more easily, which results in structures relatively more organized [44], as schematically shown in Fig. 9. The morphological effect promotes a higher porosity in thin films prepared with nanorods than in films prepared by the deposition of bipyramidal nanostructures. Particles with the isotropic structure have a dense packing [45] with fewer available active sites on the sensing layer for the reaction with the analyte, so the gas–site interaction will be more pronounced on films prepared using anisotropic nanoparticles.

Conclusions

Thin films were prepared using colloidal solutions of TiO_2 with rod and bipyramidal shapes, synthesized by a simple route in a few steps. The morphology of the nanoparticles was modulated by changing the reaction time (4, 16, and 64 h) in addition to the use of oleic acid as a surfactant, which also allowed the dispersion in an organic solvent. Employing the dip-coating method as a simple method of film deposition, it was possible to obtain thin films with a thickness around 100 nm, homogeneous morphology, and without cracks. The morphology of the nanoparticles influenced the density of the thin films, even though there was a coalescence effect during thermal treatment after the films' deposition. The films' semiconductor behavior,

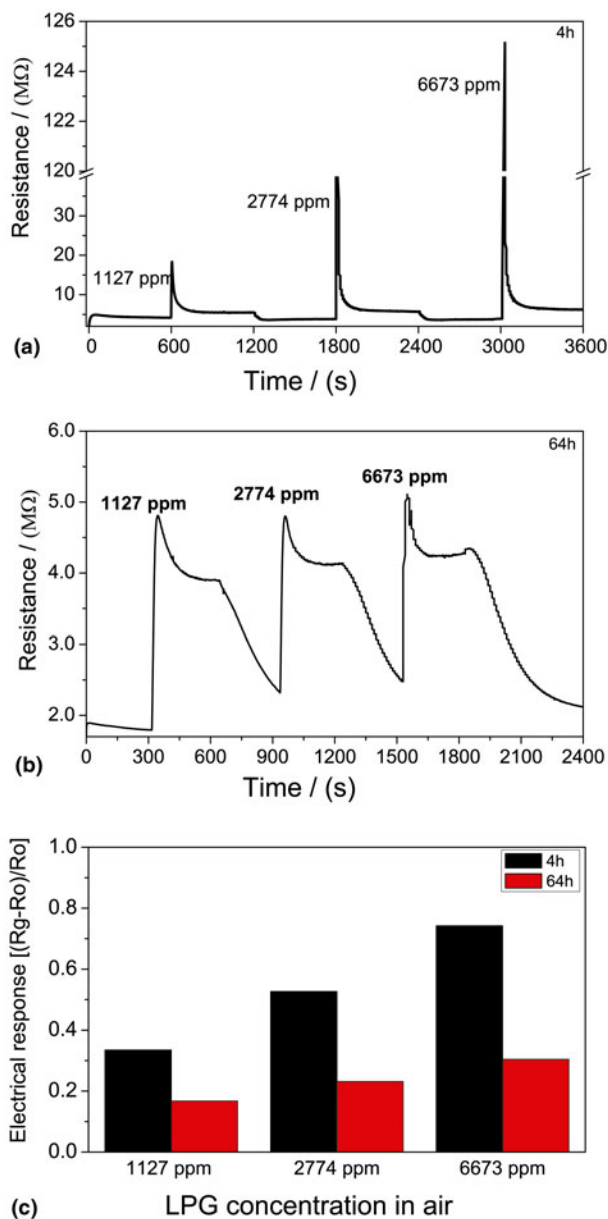


Figure 8: TiO₂ films response in the presence of different concentrations of LPG/air mixture at 350 °C (a) 4 h, (b) 64 h, and (c) electrical response of films in different LPG concentrations at 350 °C.

resistance values, and porosity influenced the platform performance in contact with LPG demonstrating that the sensitive element can be a potential gas sensor device for mixtures of air/LPG.

Experimental

Chemicals

Titanium (IV) butoxide (97%) was purchased from Sigma-Aldrich (São Paulo - SP, Brazil). Oleic acid (analytical-grade), acetone (99.5% purity), and toluene (99.8% purity)

were obtained from Synth (Diadema - SP, Brazil). All the chemical reagents were used without any further purification.

Synthesis of TiO₂

A solution of 0.25 mol/L of titanium (IV) butoxide in oleic acid was prepared. 120 mL of solution was placed in a sealed reactor (maximum useful capacity 150 mL), heated to 250 °C, and held at this temperature for different reaction times (4, 16, and 64 h). After the reaction time, the nanoparticles were washed with acetone in a relation of 1 mL per 1 mL of the reaction mixture by centrifugation at 3500 rpm for 10 min (Ionlab Daiki, model SPIN PLUS - Araucaria - PR, Brazil). The collected solid was then dispersed in toluene and washed again with acetone. The final solid was dispersed in toluene to obtain a colloidal solution with a 5 wt% of nonvolatiles.

Deposition of films

Thin films of the colloidal solution of TiO₂ nanoparticles (4 and 64 h) were deposited using a dip-coating technique onto a glass substrate (30 mm × 10 mm). The substrate was immersed in a perpendicular orientation into the colloidal solution at a rate of 8 mm/s, kept immersed for 5 s, and was then removed at the same rate as the immersion process. Next, the thin film was thermally treated in a furnace (EDG, Model 3P - São Carlos- SP, Brazil) in an air atmosphere using a heating rate of 5 °C/min, held at 500 °C for 1 h, and then cooled to room temperature using a cooling rate of 5 °C/min. Using a polished silicon substrate, thin film samples were deposited and treated under the same conditions as described for the glass substrate. These samples were used in ellipsometry measurements.

Electrical measurements

The electrical properties of the films were characterized in a sealed chamber with a controlled atmosphere and temperature. The two-point method was used using copper wires attached with a conductive silver paste over the films, and a 10 mm mask. The films were connected *via* the wires to a multimeter (Keithley model 2400 series SourceMeter, China), whereby the current-voltage curves were obtained. Thus, the response from the films was measured when mixtures of LPG/air were passed through the chamber in concentrations of 1127, 2774, and 6673 ppm of LPG. The chamber was closed (humidity: 60 ± 5%). The electrical resistance of the films was calculated by using Ohm's law ($R = V/I$). The electrical response (R) values were calculated by choosing the values of resistance from the resistance curve plateaus and using Eq. (1), where R_0 is the electrical resistance in synthetic air and R_g is the resistance value in LPG/air mixture. The resistivity values (ρ) can be obtained

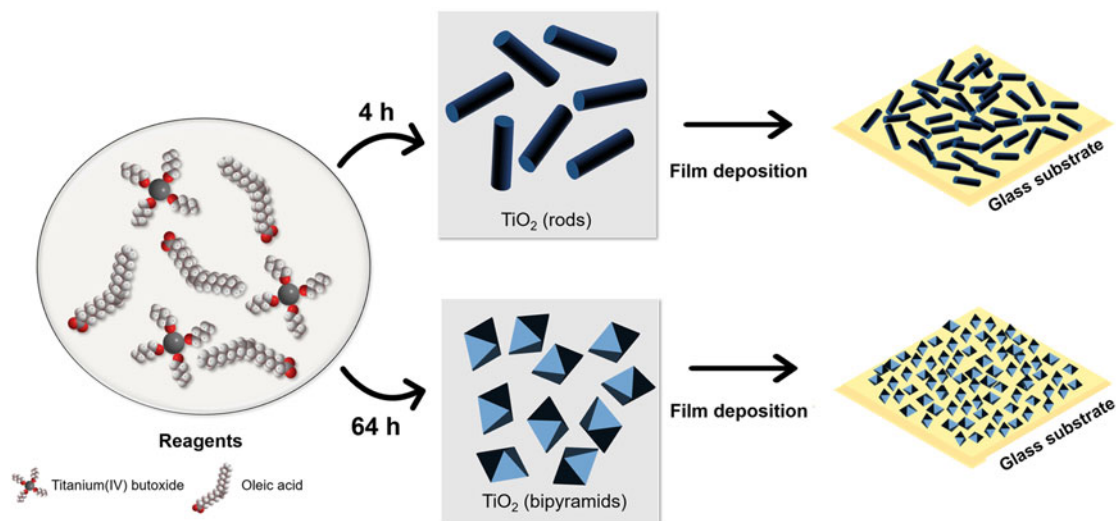


Figure 9: Nanocrystal deposition scheme in thin films obtained with different particle morphology (rods and bipyramidal).

using Eq. (2), where the values of A (area) were obtained from the average value of thickness (in SEM cross-sectional images) multiplied by substrate width, and l is the separation between the electrodes, which was 10 mm.

$$R = \frac{\Delta R}{R_0} \% = \frac{(R_g - R_0)}{R_0} \times 100, \quad (1)$$

$$\rho = R \frac{A}{l}. \quad (2)$$

Characterization techniques

X-ray diffraction

The structural phase and estimated crystallite size were evaluated from XRD data. The powder resulting from the drying of the colloidal solution and the thin films deposited on the glass substrate were analyzed by XRD in a *Rigaku model MiniFlex 600 diffractometer*, equipped with Cu anode (operating at 40 kV and 15 mA) for X-ray emission, with the predominance of the wavelength 0.154 nm, and a solid-state detector D/tex Ultra, using a step size of 0.02°.

Fourier-transform infrared spectroscopy

FTIR spectroscopy analyses were used to evaluate the organic groups bound to the surface of synthesized nanocrystals using an *Agilent Technologies Model Cary 630 FTIR spectrometer*, with attenuated total reflection accessory, operating from 4000 to 400 cm^{-1} , 128 scans and a resolution of 2 cm^{-1} .

Transmission electron microscopy

The structure and morphology of the nanocrystals were characterized by transmission electron microscopy (TEM) in an *FEI*

model Tecnai G2 F20 (Eindhoven, Netherlands), operating at 200 kV, in transmission mode. The size distribution was determined by counting at least 300 nanoparticles.

Scanning electron microscopy

The morphology of the thin films was analyzed by SEM, using an *FEI SEM F50 Inspect (Eindhoven, Netherlands)*, equipped with a field emission gun. The image was acquired in a secondary electron detector.

Ellipsometry

Thin film density was evaluated using a *Rudolph Ellipsometer AutoEL III*. For the measurements, samples were deposited on polished silicon substrates using the dip-coating technique, as previously described. The instrument was equipped with lasers (He-Ne) with a wavelength of 632.8 nm. The incidence angle was set to 70°.

Acknowledgments

The authors thank the Conselho Nacional de Desenvolvimento Científico e Tecnológico (CNPq), Fundação de Amparo à Pesquisa e Inovação do Espírito Santo (Fapes), and Federal University of Espírito Santo (Ufes) for the research funding and the scholarships.

References

1. M.S. Ahmad, A.K. Pandey, and N.A. Rahim: Advancements in the development of TiO₂ photoanodes and its fabrication methods for dye sensitized solar cell (DSSC) applications. A review. *Renew. Sustain. Energy Rev.* 77, 89 (2017).

2. L. Xu, J. Xu, H. Hu, C. Cui, Z. Ding, Y. Yan, P. Lin, and P. Wang: Hierarchical submicroflowers assembled from ultrathin anatase TiO₂ nanosheets as light scattering centers in TiO₂ photoanodes for dye-sensitized solar cells. *J. Alloys Compd.* **776**, 1002 (2019).
3. G. Kenanakis, D. Vernardou, A. Dalamagkas, and N. Katsarakis: Photocatalytic and electrooxidation properties of TiO₂ thin films deposited by sol-gel. *Catal. Today* **240**, 146 (2015).
4. J. Singh, S.A. Khan, J. Shah, R. Kotnala, and S. Mohapatra: Nanostructured TiO₂ thin films prepared by RF magnetron sputtering for photocatalytic applications. *Appl. Surf. Sci.* **422**, 953 (2017).
5. C. Lin, Y. Gao, J. Zhang, D. Xue, H. Fang, J. Tian, C. Zhou, C. Zhang, Y. Li, and H. Li: GO/TiO₂ composites as a highly active photocatalyst for the degradation of methyl orange. *J. Mater. Res.* **35**, 1307 (2020).
6. N.T.T. Thuy, D.H. Tung, L.H. Manh, J.H. Kim, S.I. Kudryashov, and P.H.J.A.S. Minh: Plasma enhanced wet chemical surface activation of TiO₂ for the synthesis of high performance photocatalytic Au/TiO₂ nanocomposites. *Appl. Sci.* **10**, 3345 (2020).
7. V. Galstyan: Porous TiO₂-based gas sensors for cyber chemical systems to provide security and medical diagnosis. *Sensors* **17**, 2947 (2017).
8. X. Li, Y. Zhao, X. Wang, J. Wang, A.M. Gaskov, and S. Akbar: Reduced graphene oxide (rGO) decorated TiO₂ microspheres for selective room-temperature gas sensors. *Sens. Actuat., B* **230**, 330 (2016).
9. J. Bai and B. Zhou: Titanium dioxide nanomaterials for sensor applications. *Chem. Rev.* **114**, 10131 (2014).
10. E. Bayan, T. Lupeiko, L. Pustovaya, M. Volkova, V. Butova, and A. Guda: Zn-F co-doped TiO₂ nanomaterials: Synthesis, structure and photocatalytic activity. *J. Alloys Compd.* **822**, 153662 (2020).
11. J. Huang and Q. Wan: Gas sensors based on semiconducting metal oxide one-dimensional nanostructures. *Sensors* **9**, 9903 (2009).
12. G. Korotcenkov: Metal oxides for solid-state gas sensors: What determines our choice? *Mater. Sci. Eng., B* **139**, 1 (2007).
13. C. Wang, L. Yin, L. Zhang, D. Xiang, and R. Gao: Metal oxide gas sensors: Sensitivity and influencing factors. *Sensors* **10**, 2088 (2010).
14. X. Chen and S.S. Mao: Titanium dioxide nanomaterials: Synthesis, properties, modifications, and applications. *Chem. Rev.* **107**, 2891 (2007).
15. D.-S. Lee, D.-D. Lee, S.-W. Ban, M. Lee, and Y.T. Kim: SnO₂ gas sensing array for combustible and explosive gas leakage recognition. *IEEE Sens. J.* **2**, 140 (2002).
16. K.R. Nemade, R.V. Barde, and S.A. Waghuley: Liquefied petroleum gas sensing by Al-doped TiO₂ nanoparticles synthesized by chemical and solid-state diffusion routes. *J. Taibah Univ. Sci.* **10**, 345 (2015).
17. N. Liu, X. Chen, J. Zhang, and J.W. Schwank: A review on TiO₂-based nanotubes synthesized via hydrothermal method: Formation mechanism, structure modification, and photocatalytic applications. *Catal. Today* **225**, 34 (2014).
18. C.J. Dalmaschio and E.R. Leite: Detachment induced by Rayleigh-instability in metal oxide nanorods: Insights from TiO₂. *Cryst. Growth Des.* **12**, 3668 (2012).
19. A.M. Alotaibi, S. Sathasivam, B.A. Williamson, A. Kafzas, C. Sotelo-Vazquez, A. Taylor, D.O. Scanlon, and I.P. Parkin: Chemical vapor deposition of photocatalytically active pure brookite TiO₂ thin films. *Chem. Mater.* **30**, 1353 (2018).
20. A.K. Haridas, B. Gangaja, P. Srikrishnarka, G.E. Unni, A.S. Nair, S.V. Nair, and D. Santhanagopalan: Spray pyrolysis-deposited nanoengineered TiO₂ thick films for ultra-high areal and volumetric capacity lithium ion battery applications. *J. Power Sources* **345**, 50 (2017).
21. A.C. Martins, A.L. Cazetta, O. Pezoti, J.R. Souza, T. Zhang, E.J. Pilau, T. Asefa, and V.C. Almeida: Sol-gel synthesis of new TiO₂/activated carbon photocatalyst and its application for degradation of tetracycline. *Ceram. Int.* **43**, 4411 (2017).
22. D. Nunes, A. Pimentel, L. Santos, P. Barquinha, L. Pereira, E. Fortunato, and R. Martins: *Chapter 2—Synthesis, Design, and Morphology of Metal Oxide Nanostructures* (Elsevier, Amsterdam, Netherlands, 2019); pp. 21–57.
23. M. Zimmermann, B. Temel, and G. Garnweitner: Parameter studies of the synthesis of titanium dioxide nanoparticles: Effect on particle formation and size. *Chem. Eng. Process.* **74**, 83 (2013).
24. M.S. Santos, J.C. Freitas, and C.J. Dalmaschio: Designed single-phase ZrO₂ nanocrystals obtained by solvothermal synthesis. *CrystEngComm* **22**, 1802 (2020).
25. E. Scopel, P.P. Conti, D.G. Stroppa, and C.J. Dalmaschio: Synthesis of functionalized magnetite nanoparticles using only oleic acid and iron (III) acetylacetonate. *SN Appl. Sci.* **1**, 147 (2019).
26. C.-S. Kim, B.K. Moon, J.-H. Park, S.T. Chung, and S.-M. Son: Synthesis of nanocrystalline TiO₂ in toluene by a solvothermal route. *J. Cryst. Growth* **254**, 405 (2003).
27. M. Niederberger and N. Pinna: *Metal Oxide Nanoparticles in Organic Solvents: Synthesis, Formation, Assembly and Application* (Springer Science & Business Media, London, United Kingdom, 2009).
28. G. Demazeau and A. Largeteau: Hydrothermal/solvothermal crystal growth: An old but adaptable process. *Z. Anorg. Allg. Chem.* **641**, 159 (2015).
29. Z. Fan, F. Meng, M. Zhang, Z. Wu, Z. Sun, and A. Li: Solvothermal synthesis of hierarchical TiO₂ nanostructures with tunable morphology and enhanced photocatalytic activity. *Appl. Surf. Sci.* **360**, 298 (2016).
30. L. Eckertová: *Mechanism of Film Formation, in Physics of Thin Films* (Springer, New York City, USA, 1977), p. 72.

31. **K.L. Chopra and I. Kaur:** *Thin Film Phenomena* (McGraw-hill, New York, 1969).
32. **R. Ortega-Borges and D. Lincot:** Mechanism of chemical bath deposition of cadmium sulfide thin films in the ammonia-thiourea system: In situ kinetic study and modelization. *J. Electrochem. Soc.* **140**, 3464 (1993).
33. **A. Chatterjee, P. Mitra, and A.K. Mukhopadhyay:** Chemically deposited zinc oxide thin film gas sensor. *J. Mater. Sci.* **34**, 4225 (1999).
34. **S.S. Lin, A. Hsieh, D.B. Min, and S.S. Chang:** A study of the color stability of commercial oleic acid. *J. Am. Oil Chem. Soc.* **53**, 157 (1976).
35. **C. Jia, T. Dong, M. Li, P. Wang, and P. Yang:** Preparation of anatase/rutile TiO₂/SnO₂ hollow heterostructures for gas sensor. *J. Alloys Compd.* **769**, 521 (2018).
36. **Y. Wang, T. Wu, Y. Zhou, C. Meng, W. Zhu, and L. Liu:** TiO₂-based nanoheterostructures for promoting gas sensitivity performance: Designs, developments, and prospects. *Sensors* **17**, 1971 (2017).
37. **B.L. Cushing, V.L. Kolesnichenko, and C.J. O'Connor:** Recent advances in the liquid-phase syntheses of Inorganic nanoparticles. *Chem. Rev.* **104**, 3893 (2004).
38. **H. Tang, K. Prasad, R. Sanjinès, P.E. Schmid, and F. Lévy:** Electrical and optical properties of TiO₂ anatase thin films. *J. Appl. Phys.* **75**, 2042 (1994).
39. **A. Hastir, N. Kohli, O.S. Kang, and R.C. Singh:** Selective liquefied petroleum gas sensor based on nanocomposites of zinc chromium oxide. *J. Electroceram.* **37**, 170 (2016).
40. **L. Hou, C. Zhang, L. Li, C. Du, X. Li, X.-F. Kang, and W. Chen:** CO gas sensors based on p-type CuO nanotubes and CuO nanocubes: Morphology and surface structure effects on the sensing performance. *Talanta* **188**, 41 (2018).
41. **N. Chen, Y. Li, D. Deng, X. Liu, X. Xing, X. Xiao, and Y. Wang:** Acetone sensing performances based on nanoporous TiO₂ synthesized by a facile hydrothermal method. *Sens. Actuat., B* **238**, 491 (2017).
42. **D. Mardare, N. Iftimie, and D. Luca:** TiO₂ thin films as sensing gas materials. *J. Non-Cryst. Solids* **354**, 4396 (2008).
43. **S. Wang, L. Pan, J.-J. Song, W. Mi, J.-J. Zou, L. Wang, and X. Zhang:** Titanium-defected undoped anatase TiO₂ with p-type conductivity, room-temperature ferromagnetism, and remarkable photocatalytic performance. *J. Am. Chem. Soc.* **137**, 2975 (2015).
44. **F. Sánchez, U. Lüders, G. Herranz, I. Infante, J. Fontcuberta, M. García-Cuenca, C. Ferrater, and M. Varela:** Self-organization in complex oxide thin films: From 2D to 0D nanostructures of SrRuO₃ and CoCr₂O₄. *Nanotechnology* **16**, S190 (2005).
45. **C.J. Dalmaschio, E.G. da Silveira Firmiano, A.N. Pinheiro, D.G. Sobrinho, A.F. de Moura, and E.R. Leite:** Nanocrystals self-assembled in superlattices directed by the solvent-organic capping interaction. *Nanoscale* **5**, 5602 (2013).